**Naval Research Laboratory**
Washington, DC 20375-5320

NRL/MR/6410--98-8303

# Numerical Modeling of Fire Suppression Using Water Mist. 4. Suppression of Liquid Methanol Pool Fires

KULDEEP PRASAD*
CHIPING LI
K. KAILASANATH

*Center for Reactive Flow and Dynamical Systems*
*Laboratory for Computational Physics and Fluid Dynamics*

**Science Application International Corporation, VA*

December 3, 1998

# REPORT DOCUMENTATION PAGE

*Form Approved*
*OMB No. 0704-0188*



| 1. AGENCY USE ONLY (*Leave Blank*) | 2. REPORT DATE | 3. REPORT TYPE AND DATES COVERED |
|---|---|---|
| | December 3, 1998 | |

4. TITLE AND SUBTITLE

Numerical Modeling of Fire Suppression Using Water Mist.
4. Suppression of Liquid Methanol Pool Fires

5. FUNDING NUMBERS

62121PE
Proj. No. MA-21-3-01

6. AUTHOR(S)

Kuldeep Prasad,* Chiping Li, and K. Kailasanath

7. PERFORMING ORGANIZATION NAME(S) AND ADDRESS(ES)

Naval Research Laboratory
Washington, DC 20375-5320

8. PERFORMING ORGANIZATION REPORT NUMBER

NRL/MR/6410--98-8303

9. SPONSORING/MONITORING AGENCY NAME(S) AND ADDRESS(ES)

Office of Naval Research
800 North Quincy Street
Arlington, VA 22217-5660

10. SPONSORING/MONITORING AGENCY REPORT NUMBER

11. SUPPLEMENTARY NOTES

*Science Application International Corporation, VA

12a. DISTRIBUTION/AVAILABILITY STATEMENT

Approved for public release; distribution unlimited.

12b. DISTRIBUTION CODE

13. ABSTRACT (*Maximum 200 words*)

This report is the fourth in a series dealing with numerical modeling of fire suppression using water mist. While the first two reports examined the interaction of water mist with two-dimensional methane air diffusion flames, the third report presented a numerical model for studying methanol liquid pool fires. As shown in that report, numerical results exhibited a flame structure that compared well with experimental observations and thermocouple temperature measurements.

In the present report we describe results for water-mist suppression of liquid methanol pool fires. The interaction of water-mist with pulsating pool fires is studied. Time dependent heat release rate profiles and temperature profiles identify the location where the water droplets evaporate and absorb energy. Numerical results are also presented for the effect of water mist on steady methanol pool fires stabilized by a strong co-flowing air jet. The relative contribution of the various suppression mechanisms such as oxygen dilution, radiation and thermal cooling on overall fire suppression is investigated. Parametric studies are performed to determine the effect of droplet injection density, velocity and droplet diameter on entrainment and overall suppression of pool fires. These results are reported in terms of reduction in peak temperature, effect on burning rate and changes in overall heat release rate. Numerical simulations indicate that small droplet diameters exhibit smaller characteristic time for decrease of relative velocity with respect to the gas phase, and therefore entrain most rapidly into the diffusion flame. Hence for the co-flow injection case, smaller diameter droplets produce maximum flame suppression for a fixed amount of injection spray density.

14. SUBJECT TERMS

Fire Suppression
Liquid pool fire combustion

15. NUMBER OF PAGES

27

16. PRICE CODE

| 17. SECURITY CLASSIFICATION OF REPORT | 18. SECURITY CLASSIFICATION OF THIS PAGE | 19. SECURITY CLASSIFICATION OF ABSTRACT | 20. LIMITATION OF ABSTRACT |
|---|---|---|---|
| UNCLASSIFIED | UNCLASSIFIED | UNCLASSIFIED | UL |

NSN 7540-01-280-5500

Standard Form 298 (Rev. 2-89)
Prescribed by ANSI Std 239-18
298-102

## CONTENTS

## LIST OF FIGURES

# Numerical Modeling of Fire Suppression using Water Mist. 4. Suppression of Liquid Methanol Pool Fires

## 1. INTRODUCTION

Water mist suppression of liquid pool fires [1]- [4] has been studied for at least 50 years. Recent research in water mist technology has been driven by two events:

- The phase out of Halon 1301 ($CF_3Br$) and the search for alternative technologies that preserve most of the benefits of a clean total flooding agent without the adverse environmental impact.
- International Maritime Organization (IMO) regulations requiring retrofit of fire suppression systems on most commercial marine vessels.

This report is the fourth in a series dealing with the numerical modeling of fire suppression using water mist. In the first report [5], a numerical study was described for obtaining a detailed understanding of the physical processes involved during the interaction of water-mist and methane-air diffusion flames. The relative contribution [6] of the various suppression mechanisms was studied and detailed comparison with experimental results was provided. The second report [7] described a computational study for optimizing water-mist injection characteristics for suppression of co-flow diffusion flames. The effect of droplet diameter, mist injection angle (throw angle), mist density and velocity on water-mist entrainment into the flame and flame suppression were quantified [8]. Numerical results were presented for symmetric and asymmetric spray pattern geometries resulting from base injection and side injection nozzle orientation.

The focus of the third report [9] was on numerical modeling of methanol liquid pool fires. A mathematical model was described to simulate the evaporation and burning of liquid methanol. The complete set of unsteady, compressible Navier-Stokes equations were solved in the gas phase to describe the advection of the fuel gases away from the pool surface, diffusion of the gases into the surrounding air and the oxidation of the fuel molecules into product species. Heat transfer into the liquid pool and the metal container through conduction, convection and radiation were modeled by solving a modified form of the energy equation. Clausius-Clapeyron relationships were invoked to model the burning rate of a two-dimensional pool of pure liquid methanol [10]. The governing equations along with appropriate boundary and interface conditions were solved using the flux corrected transport model. Numerical results exhibited a flame structure that compares well with experimental observations.

In the present report we describe results for water-mist suppression of liquid methanol pool fires. The interaction of water-mist with pulsating and steady pool fires is studied. Time dependent heat release rate profiles show the location where the water droplets evaporate and absorb energy. A series of parametric studies are performed to determine the effect of droplet number density,

Manuscript approved October 28, 1998.

injection velocity and diameter on entrainment and overall suppression of pool fires. These results are reported in terms of reduction in peak temperature, effect on burning rate and changes in overall heat release. The relative contribution of various suppression mechanisms such as oxygen dilution, radiation and thermal cooling on flame inhibition is also studied in detail.

In the following sections, we briefly describe the mathematical and numerical model for simulating the burning of methanol liquid pool fires and the suppression of these fires using water droplets. The major portion of this report describes interaction of water droplets with pulsating pool fires as well as steady pool fires stabilized by a co-flowing air jet. Droplet sectional density contours are used to identify the location where the droplets evaporate and absorb energy from the diffusion flame. The effect of injection density, droplet diameter and injection configuration on water mist entrainment into the flame and overall flame suppression has also been discussed in detail in the section dealing with results and discussion.

## 2. MATHEMATICAL AND NUMERICAL MODELS

The mathematical models for studying liquid pool fires has been discussed in reference [9], [10]. These mathematical models describe the various physical processes occurring during the evaporation of the liquid pool, the convection, diffusion and the chemical reactions between the gaseous fuel and the oxidizer and the entrainment of air into the flame.

The energy release in the gas phase due to the exothermic chemical reactions between the fuel and entrained oxygen heats up the methanol liquid pool. This raises the temperature of the pool close to the boiling point temperature of the fuel. Thermal conduction transfers some of the energy away from the pool surface and heats up the layers of liquid methanol below the surface. As the liquid evaporates fresh fuel is introduced through the bottom of the pool to maintain the surface of the pool at a certain level. It is assumed that the liquid only has a velocity component normal to the gas-liquid interface. The horizontal velocity component is assumed to be zero. Heat conduction in the liquid phase occurs in both the x and y directions. Assuming no chemical reactions in the liquid methanol pool, an energy conservation equation can be formulated for the pool as discussed in reference [9], [10]. The burning rate is iteratively changed until the local vapor pressure of methanol gas above the pool surface is equal to the computed Clausius-Clapeyron pressure.

Detailed modeling of gas-phase reacting flows is based on a generally accepted set of time dependent coupled partial differential equations maintaining conservation of total mass, momentum, total energy and individual species density [5]- [10], [11]. These equations describe the convective motion of the fluid, the chemical reactions among the constituent species and the diffusive transport processes such as thermal conduction and molecular diffusion. A strong conservation form of the two-dimensional, unsteady, compressible Navier-Stokes equations is used to describe gas phase reactive flow systems. Allowances are made for variable thermal and transport properties [12]. A single step reaction mechanism is employed to model the oxidation of methanol gas using a quasi-global Arrhenius expression. Since methanol is a relative low sooting fuel, the optically thin assumption is used in the radiation transport sub model. Configuration factors are computed to determine the fraction of radiative energy that is absorbed by the methanol fuel to the total radiative energy emitted by the hot gases. A Beer's law model is further used to describe the reduction in beam irradiance brought about by absorption in the liquid phase [9], [10].

In order to study the interaction between water-mist and fires, a two-continuum formulation

is used in which the gas phase and the water mist are both described by equations of the Eulerian form. It is assumed that coalescence and breakup of droplet properties are insignificant within the computational domain. In practical sprays, the actual number of discrete droplet sizes can be immense. A sectional conservation model is employed which avoids the dimensionality problem associated with the discrete form of the droplet population balance equation. This method is based on dividing the droplet size domain into sections and dealing only with one integral quantity in each section. This sectional representation has the advantage that the integral quantity is conserved within the computational domain and the number of conservation equations is substantially reduced so as to equal the number of sections. Each of the droplet sections is assumed to have its own unique velocity different from that of the gas phase. Momentum conservation equations are formulated for each droplet section and are coupled to those of the gas phase through the phase interaction terms (drag terms). The interphase drag force experienced by the two phases is related to the particle Reynolds number by a drag coefficient $C_D$ [5]- [8].

The governing equations are rewritten in terms of finite volume approximations on an Eulerian mesh and solved numerically using a time marching procedure [11]. The fluid convection is solved using a high order implicit algorithm, Barely Implicit Correction to the Flux Corrected Transport (BIC-FCT) [13] that was developed to solve the convection equations for low-velocity flows. The Flux-Corrected Transport (FCT) algorithm [14] itself is an explicit, finite difference algorithm that is constructed to have fourth order phase accuracy. The solution approach consists of separate algorithms for each of the individual processes, which are coupled together by the method of fractional time-step splitting. The algorithms for convection, thermal conduction, molecular diffusion, chemical reactions and the coupling of the individual processes have been previously discussed in detail [5]- [10].

## 3. RESULTS AND DISCUSSION

Figure 1 is a schematic diagram of a two-dimensional methanol pool burner geometry. The figure also shows some of the important physical processes involved in the evaporation and combustion of liquid methanol. The fluid dynamic equations, describing the gas and the liquid phase, presented earlier were solved using the numerical methodology briefly discussed above, to study the suppression of two-dimensional liquid methanol pool fires stabilized above a Wolfhard Parker diffusion flame burner.

### 3.1 Suppression of Pulsating Pool Fires

Numerical simulations have been performed to study the various physical processes involved during the suppression of a pulsating methanol pool fire. Calculations were performed on a 2-dimensional methanol pool with a half thickness of 0.5 cm and an air co-flow velocity of 10 $cm/sec$. The typical temperature ($^oK$) and heat release rate contours ($J/m^3/sec$) without water mist were shown in reference [9]. The heat release rate contours indicate the region of rapid exothermic chemical activity. This profile also identifies the location of the flame sheet where the fuel and oxidizer species come together in stoichiometric proportions, react exothermically and produce product species. The heat release rate contours indicate the presence of a thin flame sheet which closes above the fuel duct. The vorticity contours presented in reference [9] clearly show the presence of coherent vortical structures which are shed by the fire periodically. We now inject $50\mu m$ water mist droplets at the base of the diffusion flame with a droplet injection density of

$1000 drops/cm^3$ and an initial injection velocity of 25 $cm/sec$. Figure 2 shows the time-dependent heat release rate profiles for water-mist suppression of methanol pool fires. The red region indicates very high exothermic chemical activity whereas the blue region represents endothermic contours. The endothermic regions show the location where the water-mist evaporates and absorbs energy from the diffusion flame. It should be noted that the location where the droplets evaporate and absorb energy from the diffusion flame changes as a function of time. This is because as the vortical structures periodically convect away from the pool surface they change the rate of air entrainment into the flame. This in turn affects the entrainment of water-mist into the flame and consequently the location where heat extraction takes place.

Figure 3 shows typical time dependent temperature contours for water-mist suppression of methanol pool fires. The maximum flame temperature reduces from $1840K$ for the base case flame (no water mist) to $1795K$ for the case with water-mist. Since the basic flame is pulsating in nature, it is difficult to observe changes in flame shapes due to addition of water mist. We observe that the fire in the presence of water-mist exhibits features similar to an un-suppressed fire. It still exhibits a fuel rich core (persistent zone), an intermittent region with a time varying visible flame tip and a downstream plume region. These regions were also observed for the un-suppressed fire as discussed in reference [9] and compared with experimental results from McCaffrey [15]. The average shedding frequency for the base case flame without water mist was found to be approximately 12 $Hz$. When subjected to water-mist the puffing frequency increases to 13.5 $Hz$. Further work is needed to study the effect of increasing the injection density on the average shedding frequency.

The injected spray is a mono-disperse spray and consists entirely of $50\mu m$ droplets. These droplets convect along with the air co-flow. Some of these droplets evaporate and form smaller droplet sections while others convect out of the computational domain. To keep track of the droplets of different sizes, the droplets are divided into five sections as follows : $0-10\mu m$, $10-20\mu m$, $20-30\mu m$, $30-40\mu m$ and $40-50\mu m$. The droplets that entrain into the diffusion flame evaporate and form smaller sections, resulting in a very distinct cascading effect, in which larger diameter droplets show maximum concentration further away from the diffusion flame, and smaller diameter droplets show maximum concentration closer to the diffusion flame. Figure 4 shows the time dependent sectional densities for the $0-10\mu m$ section. The higher droplet section densities indicate the regions where the droplets evaporate and absorb energy from the diffusion flame.

Simulations were also performed with $150\mu m$ droplets injected at the base of the diffusion flame with an initial injection velocity of 25 $cm/sec$. In this case the droplets are divided into five sections consisting of $0-30\mu m$, $30-60\mu m$, $60-90\mu m$, $90-120\mu m$ and $120-150\mu m$. Unlike the case with $50\mu m$ droplets the larger droplet sections for the $150\mu m$ case were unable to convect too far above the burner surface. The drag force acting on these droplets is not able to counter balance the weight of these droplets and as a result the droplet velocity continuously reduces.

### 3.2 Suppression of Steady Pool Fires

Due to the unsteady nature of the pulsating pool fire it is difficult to study the details of the interaction of water-mist with the pool fire. Therefore, to stabilize the pool fire, the air co-flow velocity was increased to 40 $cm/s$. When the air co-flow velocity was increased, the vortical structures are pushed further away from the burner surface. Reference [9] shows temperature and heat release rate contours above a methanol pool fire stabilized by a strong co-flowing air jet.

Numerical simulations were then performed to ascertain the effect of changing the injection spray density on these steady pool fires. Figure 5 shows temperature contours for various spray injection densities of 1000, 3000, 5000 and 9000 $drops/cm^3$ of $50\mu m$ water mist droplets. As in the previous simulations, the spray is injected along with the air co-flow perpendicular to the burner surface with an initial injection velocity of 25 $cm/s$. As the spray injection density increases, the flame becomes taller and broader (fatter), resulting in larger flame surface area. The flame height increases from 3.5 $cm$ for the base case flame to about 4.5 $cm$ for the 3000 $drops/cm^3$ case and to 7.0 $cm$ for the 9000 $drops/cm^3$ case.

Figure 6 shows typical heat release rate contours for suppression of steady pool fires subjected to water mist. The water-mist is injected at the base of flame with an initial injection density of 3000 $drops/cm^3$ and an initial injection velocity of 25 $cm/s$. The heat release rate profile indicates the presence of an endothermic heat release rate profile (negative value) showing the approximate location of evaporation of the droplets. The sectional density contours for $0-10\mu m$, $20-30\mu m$ and $40-50\mu m$ sections have been shown in Figure 7 illustrating the movement of the various droplet sections.

### 3.3 Effect of Droplet Diameter and Injection Density

A series of parametric studies were performed to estimate the effect of droplet number density and droplet mass density on flame suppression and flame extinction. Figure 8 shows changes in peak temperature as a function of droplet mass density. Numerical simulations were performed with 50 and $150\mu m$ droplets with varying levels of injection spray density. The injection velocity of the droplets was unchanged in these calculations. The peak temperature observed for each simulation was mapped as a function of droplet number and mass densities. The profiles of peak temperature vs. droplet injection mass density indicate that as the droplet mass density increases, the flame temperature reduces until a certain critical mass density is reached beyond which point a stable flame cannot be sustained. This trend was observed for all water mist droplet diameters studied in this analysis. It is also observed that as the droplet diameter increases, the injection spray mass density required to produce the same amount of suppression also increases. Thus in a co-flow configuration, smaller diameter mist droplets result in better and more efficient suppression for the same injection mass density. Peak temperature as a function of injection number density (Figure 9) show that the trends (as observed in Figure 8) are reversed. This figure shows that the larger diameter droplets produce more effective suppression for a fixed inlet injection number density. This is because when the injection number density is held fixed, larger diameter droplets result in larger amount of mass entrained into the flame as compared to smaller diameter droplets.

### 3.4 Effect of Water Mist on Average Burning Rate

Figure 8 also shows variation in average burning rate $r_b$ as a function of mist flow rate. The average burning rate is obtained by first integrating the local burning rate over the entire pool surface to give the total burning rate and then dividing the total burning rate by the pool surface area [9]. We observe an average burning rate of 36 $\mu m/s$ for the base case with no mist flow rate. For the case of $50\mu m$ droplets we observe that the average burn rate stays approximately constant at a value of 36 $\mu m/s$ as the mist flow rate increases. For a mist flow rate of 0.5 $kg/m^2/s$ we observed that the burning rate suddenly reduces to zero and the flame was extinguished. For the $150\mu m$ droplets we observe that the burning rate increases to 37 $\mu m/s$ for a mist flow rate of 0.4

$kg/m^2/s$. We also observe that the average burning rate abruptly goes to zero for a mist flow rate greater than 1.0 $kg/m^2/s$. The slight increase in average burning rate is attributed to changes in vapor pressure of gaseous methanol at the pool surface due to the addition of water-mist. We also observe that the exact location of the abrupt drop in average burning rate is relatively insensitive to small changes in the Arrhenius parameters that were chosen to model the oxidation of methanol gas.

The factors that control the average burning rate of a pool of liquid methanol include

- Heat feedback from the hot gases to the liquid pool.
- Vapor pressure of gaseous methanol at the pool surface.
- Temperature of the pool surface.

A combination of these three factors determines the rate of burning of liquid methanol. We believe that when water-mist is injected at the base of the diffusion flame, it is gradually entrained into the flame along with the air. As a result the flame very close to the pool surface is not cooled as much as portions of the flame that are further away from the pool surface. This results in negligible changes in heat feedback or temperature gradient at the pool surface due to the addition of water mist. Although the temperature gradient is smaller than that for the case without water mist, the reduction in burning rate is relatively small. The presence of water mist however changes the vapor pressure of methanol gas and this in turn may result in slightly higher burning rate in order for the Clausius-Clapeyron pressure to be equal to the vapor pressure. The third factor is the change in temperature of the pool surface due to the addition of water mist and heat losses from the pool surface due to cooling of the metal walls. This will have an additional effect on the average burning rate. More detailed studies on the effect of changes in pool surface temperature due to the addition of water mist need to be carried out to fully understand its impact on the average burning rate.

### 3.5 Mechanisms of Flame Suppression

There are four major mechanisms involved in the extinction/suppression of pool fires by water mist. These include thermal cooling, oxygen displacement, fuel surface cooling and radiation attenuation. When flames are subjected to water-mist, water droplets evaporate by absorbing energy from the flame [5], [6]. This effect of the latent heat of evaporation is included in the "thermal cooling" effect. Once the droplets evaporate, they produce water vapor which dilutes the oxidizer of the surrounding air flow. This oxygen displacement further suppresses the fire because of changes in the rates of exothermic chemical reactions due to changes in density of the reactants. The water vapor, due to its larger heat capacity as compared to air, can also change the specific heat of the reactant gases resulting in further suppression of the flame. All these effects, other than those associated directly with the latent heat of evaporation are included in the "oxygen displacement effect".

Radiation attenuation occurs when the presence of water-mist changes the net radiation reaching the fuel surface and as a result affects the heat feedback to the fuel surface and the fuel surface temperature. The resulting flame suppression is accounted to be due to radiation attenuation. Fuel surface cooling occurs when water-mist falls on the fuel surface and absorbs energy from the fuel surface resulting in lowering of the temperature of the fuel surface and subsequent changes in the burning rates. Since water-mist dissolves in the methanol pool, this may also change the concentration of methanol that is evaporating from the pool surface and may result in additional

flame suppression. It should be noted that fuel surface cooling may also occur indirectly because of thermal cooling, oxygen displacement and radiation. These effects may result in lower flame temperatures or lower heat feedback to the pool surface resulting in cooling of the fuel surface. In the present analysis, we do not allow for the water-mist to dissolve into the liquid pool and as a result we do not account for the direct method of fuel surface cooling. However we do allow for the fuel surface to cool indirectly due to changes in flame temperature and heat feedback. Flame suppression due to this indirect fuel surface cooling is also assumed to be part of the mechanism that caused the surface temperature to change. Thus if oxygen dilution changes the flame temperature and heat feedback to the fuel surface, which in turn changes the fuel surface temperature, the resulting flame suppression is also assumed to be a part of the oxygen dilution effect.

Let us consider the case of $50\mu m$ droplets injected along with the air co-flow at a velocity of 25 $cm/sec$ and an initial spray density of 3000 $drops/cm^3$. Figure 10 (Case a) shows the temperature contours for the base case diffusion flame whereas Figure 10 (Case b) shows the temperature contours for the case with water mist. This simulation contains the suppression effect due to thermal cooling, oxygen dilution and radiation. When water droplets are introduced into the flame (Case b), the flame appears to cool down significantly. The flame also appears to become taller and broader. The numerical simulation was repeated with zero value for the heat of evaporation. The resulting temperature contours have been shown in Figure 10 (Case c). This case illustrates the effect of dilution and radiation. We observe that the flame is cooler than the flame in a) but hotter than b). The flame for case c is even taller than case b and case a. Numerical simulations were next performed with zero value for the heat of evaporation as well as no radiative heating of the fuel surface. Although the flame is allowed to loose heat by radiation, in these simulation we do not allow this heat to be absorbed at the fuel surface. Figure 10 (Case d) shows temperature contours for the case where both radiative heating of the fuel surface is absent and the heat of evaporation is set to zero. This case represent the pure effect of oxygen displacement. Finally (Case e) shows temperature contours for water mist suppression of pool fires but without the radiation terms. This case contains the effect of dilution as well as thermal cooling.

Figure 11 shows temperature profiles at a height of 3, 6, 9 and 12 $mm$ above the pool surface for the five cases discussed above. Our results indicate that close to the pool surface thermal cooling has a huge effect on flame suppression, while oxygen displacement is a relatively small effect. As we move above the pool surface the effect of oxygen displacement increases. At a height of 12 mm above the burner surface, we find that oxygen displacement is equally important for flame suppression as is thermal cooling. It should be noted that the flame heights and flame shapes for the various cases is significantly different and is not taken into account when the temperature profiles are compared at a certain height above the pool surface. It was found that radiation has a very small effect on flame suppression. This result may only be applicable to small scale pool fires. For larger scale pool fires, we expect radiative losses to play a more significant role in flame suppression.

### 3.6 Degree of Entrainment

Figure 12 shows the centerline $H_2O$ gas density for various spray injection densities of $50\mu m$ droplets. This figure also shows the base case centerline $H_2O$ gas density profile. Since water mist is absent in the base case calculation, this density value is purely due to convection and diffusion of water-vapor produced during chemical reactions alone. The difference between the spray injection

density profile and the base case profile gives a rough measure of the amount of $H_2O$ gas entrained into the flame. As expected, it is found that as the spray injection density increases the amount of mist entrained into the flame also increases for a given initial droplet diameter. Figure 13 shows the centerline temperature profiles for various spray injection densities. The droplet diameter and droplet velocity are the same as for the case shown in Figure 12. As the droplet density increases, the centerline temperature reduces and this difference in temperature represents the net suppression due to a combined effect of thermal cooling and oxygen dilution. It should be noted that temperature reduction at the centerline is negligibly small in the first 1.0 $cm$ above the liquid pool surface, but then increases with height.

### 3.7 Optimization Study

The net suppression due to water mist and the impact of droplet diameter and injection density have been summarized in Figure 14. The abcissa of this figure shows the net amount of water mist injected per unit mass flow rate of fuel (base case), whereas the ordinate is a ratio of the integrated heat release in the computational domain with water mist ($\Delta H_T$) to the integrated value without water mist ($\Delta H_0$). This ratio therefore represents a net integrated measure of the suppression of a flame. Efficient design of water mist systems aims at obtaining the maximum amount of suppression with the minimum amount of water mist added to the system; that is to minimize the value of the abcissa and the ordinate. Figure 14 shows results for sprays with initial injection droplet diameter of $50\mu m$ and $150\mu m$. For each droplet diameter the net suppression increases with spray density. Overall our results indicate that for the co-flow configuration, smaller diameter droplets provide maximum suppression for the minimum spray mass density.

Computations were carried out with water-mist injection directed at an angle of $45^0$ to the pool surface for a wide range of droplet diameters, injection densities and spray velocities. Although both symmetric and asymmetric geometries were considered, only results for symmetric configuration have been shown in this report. Symmetric injection refers to water-mist injection that is directed towards the diffusion flame from both sides of the flame. Figure 14 shows the net suppression effect of water-mist injected along with the air co-flow at the base of the diffusion flame at an angle of $45^0$ to the burner surface (solid line with circles). Along each curve the droplet injection density is progressively increased, but the droplet diameter, injection velocity and angle are maintained constant. Results indicate that the degree of flame suppression increases with larger mist flow rates. We also observe that for a given mist flow rate, injection at an angle of $45^0$ to the pool surface produces larger suppression than injection at an angle of $90^0$ to the pool surface (Base case). The differences in the degree of suppression between the base case and injection at $45^0$ angle become larger with higher injection velocities.

Numerical simulations have also been performed with water-mist injection from the top of the computational domain (top injection configuration). The net suppression due to top injection has been shown in Figure 14 for initial droplet diameters of $50\mu m$ and $150\mu m$ (diamond symbols). For the top injection configuration we find that the degree of suppression is extremely small as compared to the base injection configuration. This is because in the top injection configuration, the droplets had to flow in a direction opposite to the the hot gases in the plume (which are flowing at a very high speed) that are flowing out of the computational domain. The $50\mu m$ droplets are unable to overcome the drag force exerted by these gases and never reach close to the diffusion flame. The $150\mu m$ droplets are able to travel further towards the diffusion flame because of the

higher momentum associated with these droplets. In either case the degree of suppression was extremely small. The $150\mu m$ droplets show slightly more suppression than the $50\mu m$ droplets. We believe that for the top injection configuration, water mist will have to be injected at very high speeds to overcome the drag force exerted by the plume gases and travel the large distance separating the point of injection and the diffusion flame.

The top injection configuration was also studied with pool fires with very small co-flow air velocities. When the air co-flow velocity is very small the droplets that are injected from the top are able to travel further towards the diffusion flame (under the force of gravity). However under these conditions the flame itself is a time dependent pulsating flame. This results in a degree of suppression that varies with time and is no longer a constant value. As a result it is very difficult to show these results on Figure 14.

## 4. CONCLUSIONS

Numerical simulations have been presented for the evaporation and burning of small scale methanol pool fires and their inhibition by water mist. The complete set of unsteady compressible Navier-Stokes equations are solved for studying methanol fires stabilized above a two-dimensional liquid pool. Both the gas phase and water mist are described by equations of the Eulerian form. An energy equation is solved within the liquid pool to model the evolution of the thermal wave and Clausius-Clapeyron relations are employed to model the burning rate. The model has been validated by comparing temperature profiles and burning rate with experimental data. Numerical simulations have been performed to identify the relative contribution of the various suppression mechanisms. Results indicate that close to the pool surface, thermal cooling has a huge effect on flame suppression, while oxygen displacement is a relatively small effect. However, as we move further away from the pool surface, oxygen displacement becomes equally important for flame suppression as thermal cooling. Parametric studies were completed to evaluate the effect of droplet diameter, injection density and velocity on mist entrainment and overall fire suppression. It was observed that smaller droplets entrain most rapidly into the pool fire for the co-flow injection case and hence produce maximum suppression for a fixed amount of injection spray density. It was also observed that injection at an angle of $45^0$ to the pool surface resulted in better flame suppression as compared to base injection. We also observe that under top injection configuration, the droplets are unable to overcome the drag force exerted by the plume gases and this results in lower suppression as compared to the base injection configuration.

## 5. ACKNOWLEDGEMENT

The work described in this report was performed by the Laboratory for Computational Physics and Fluid Dynamics of the Materials Science and Component Technology Directorate, Naval Research Laboratory. The work was funded by the Office of Naval Research, Code 334, under the Damage Control Task of the FY98 BA2 Surface Ship Hull, Mechanical and Electrical Technology Program (PE0602121N).

## 6. REFERENCES


1. Hall, A. R., Oxidation and Combustion Review, 6, 169 (1973).
2. Hamins, A., Kashiwagi, T. and Buch, R., *Characteristics of Pool Fire Burning*, Fire Resistance of Industrial Fluids, ASTM STP 1284, George E. Totten and Jurgen Reichel, Eds. American Society for Testing and Materials, Philadelphia (1995).
3. Joulain, P., *The Behavior of Pool Fires : State of the Art and New Insights*, Twenty-seventh Symposium (International) on Combustion (1998).
4. Hottel, H. C., Fire Research Abstract Reviews, 1, 41 (1959).
5. Prasad, K., Li, C., Kailasanath, K., Ndubizu, C., Gopal, R. and Tatem, P.A.,*Numerical Modeling of Fire Suppression Using Water Mist. 1. Gaseous Methane-Air Diffusion Flame*, Naval Research Laboratory, Memorandum Report, NRL/MR/6410-98-8102 (1998).
6. Prasad, K., Li, C., Kailasanath, K., Ndubizu, C., Gopal, R. and Tatem, P.A., *Numerical Modeling of Water Mist Suppression of Methane-Air Diffusion Flame*, Comb. Sci. & Tech., V. 132, 1-6, p-325 (1998).
7. Prasad, K., Li, C. and Kailasanath, K., *Numerical Modeling of Fire Suppression Using Water Mist. 2. An Optimization Study on Jet Diffusion Flames*, Naval Research Laboratory, Memorandum Report, NRL/MR/6410-98-8159 (1998).
8. Prasad, K., Li, C. and Kailasanath, K., *Optimizing Water-mist Injection Characteristics for Suppression of Co-flow Diffusion Flames*, Twenty-seventh Symposium (International) on Combustion (1998).
9. Prasad, K., Li, C., Kailasanath, K., Ndubizu, C., Gopal, R. and Tatem, P.A., *Numerical Modeling of Fire Suppression Using Water Mist. 3. Methanol Liquid Pool Fire Model*, Naval Research Laboratory, Memorandum Report, NRL/MR/6410-98-8190 (1998).
10. Prasad, K., Li, C., Kailasanath, K., Ndubizu, C., Gopal, R. and Tatem, P.A., *Numerical Modeling of a Methanol Liquid Pool Fire*, submitted, Combustion Theory and Modeling (1998).
11. Oran E.S. and Boris, J. P., *Numerical Simulation of Reactive Flow*, Elsevier Publication (1987).
12. Kailasanath, K., Oran, E.S. and Boris, J.P., NRL Memorandum Report, 4910 (1982).
13. Patnaik, G., Guirguis, R. H., Boris, J. P. and Oran, E.S., *A Barely Implicit Correction for Flux Corrected Transport*, Journal of Computational Physics, 71:1-20 (1987).
14. Boris, J.P., and Book, D.L., *Flux Corrected Transport I. SHASTA, A Fluid Transport Algorithm That Works*, Journal of Computational Physics, 11 (1) pp.38-69 (1973).
15. McCaffrey, B. J., Center for Fire Research, NBSIR 79:1910 (1979).

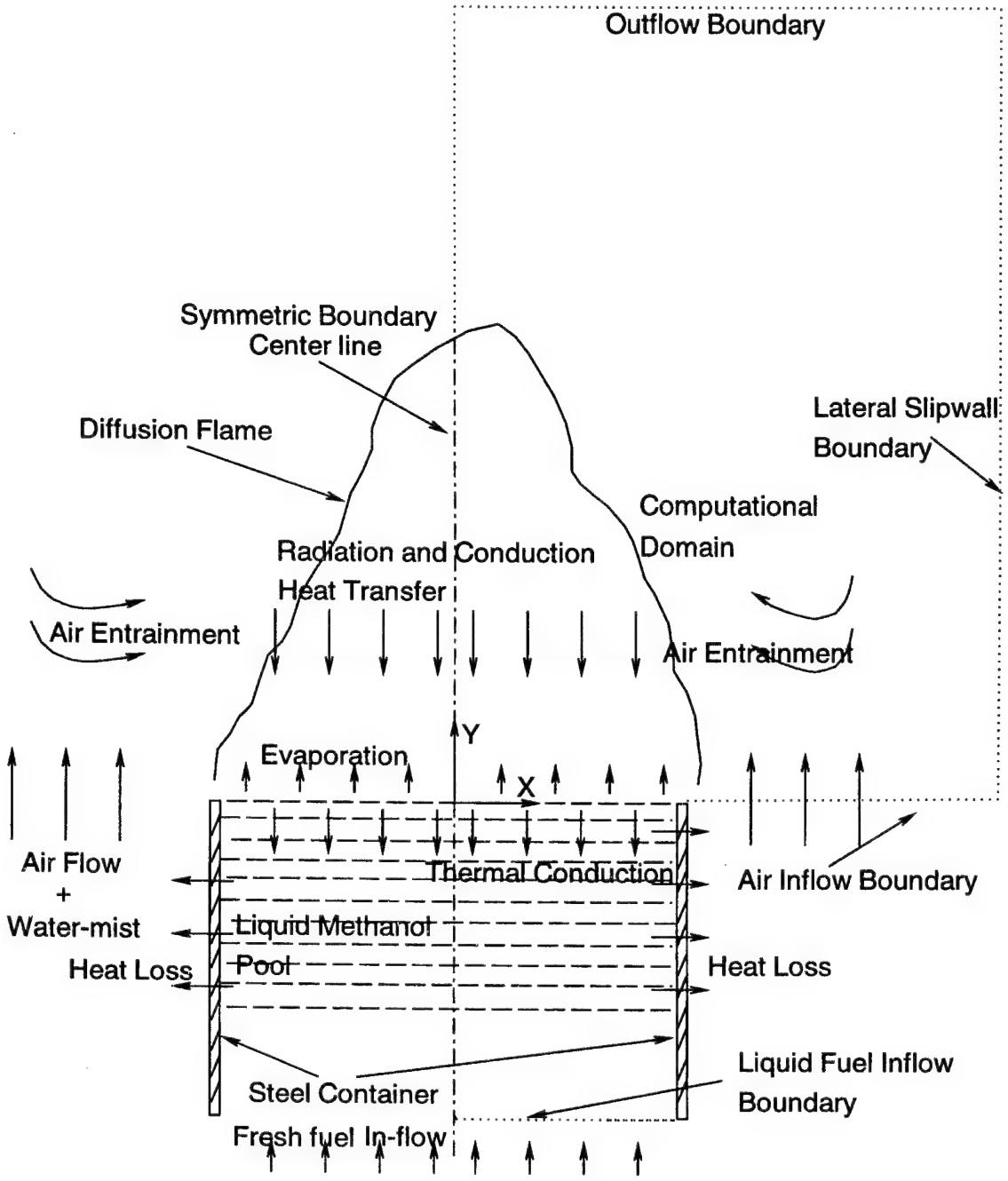


Fig. 1. Schematic diagram of a methanol liquid pool fire burner geometry. The gas phase and the liquid phase computational domain in which the solutions are desired have been shown along with some of the physical processes involved during the evaporation of liquid methanol.

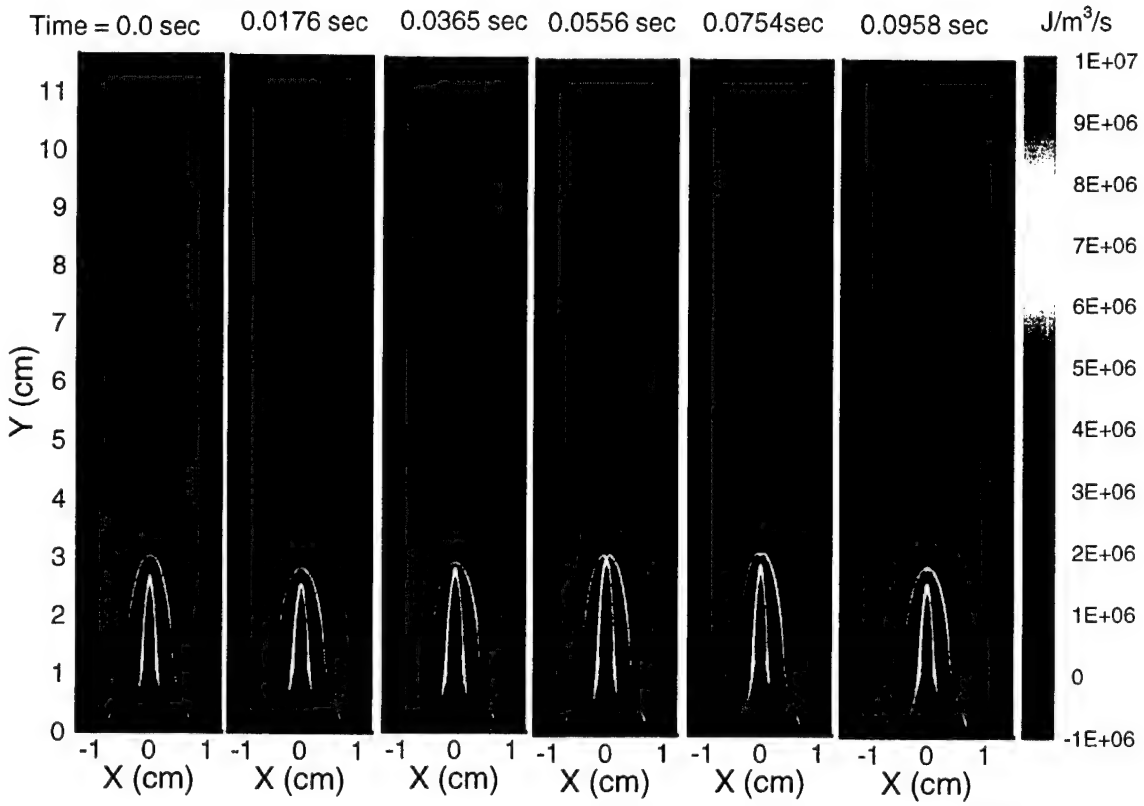


Fig. 2. Time dependent heat release rate profiles for water-mist suppression of methanol pool fire with an air co-flow velocity of 10 $cm/s$. The water-mist ($50\mu$ , 1000 $drops/cm^3$) is injected at the base of the flame.

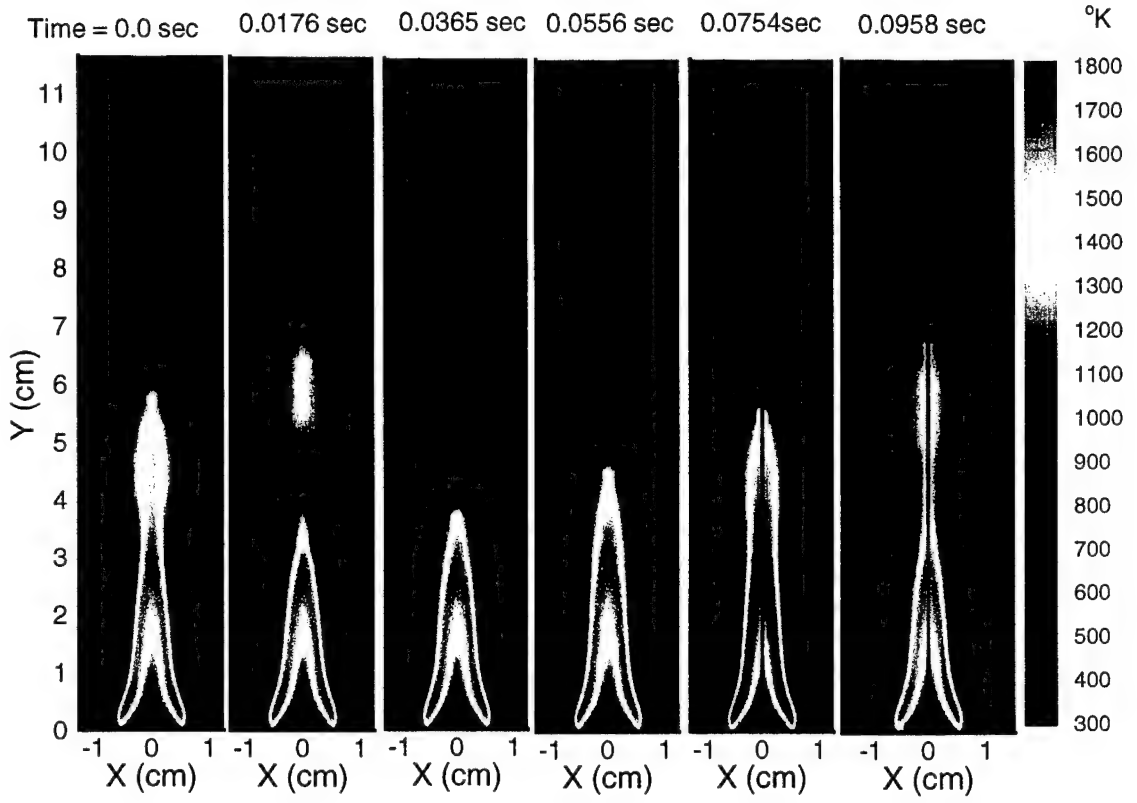


Fig. 3. Time dependent temperature profiles for water-mist suppression of methanol pool fire with an air co-flow velocity of 10 $cm/s$. The water-mist ($50\mu$ , 1000 $drops/cm^3$) is injected at the base of the flame.

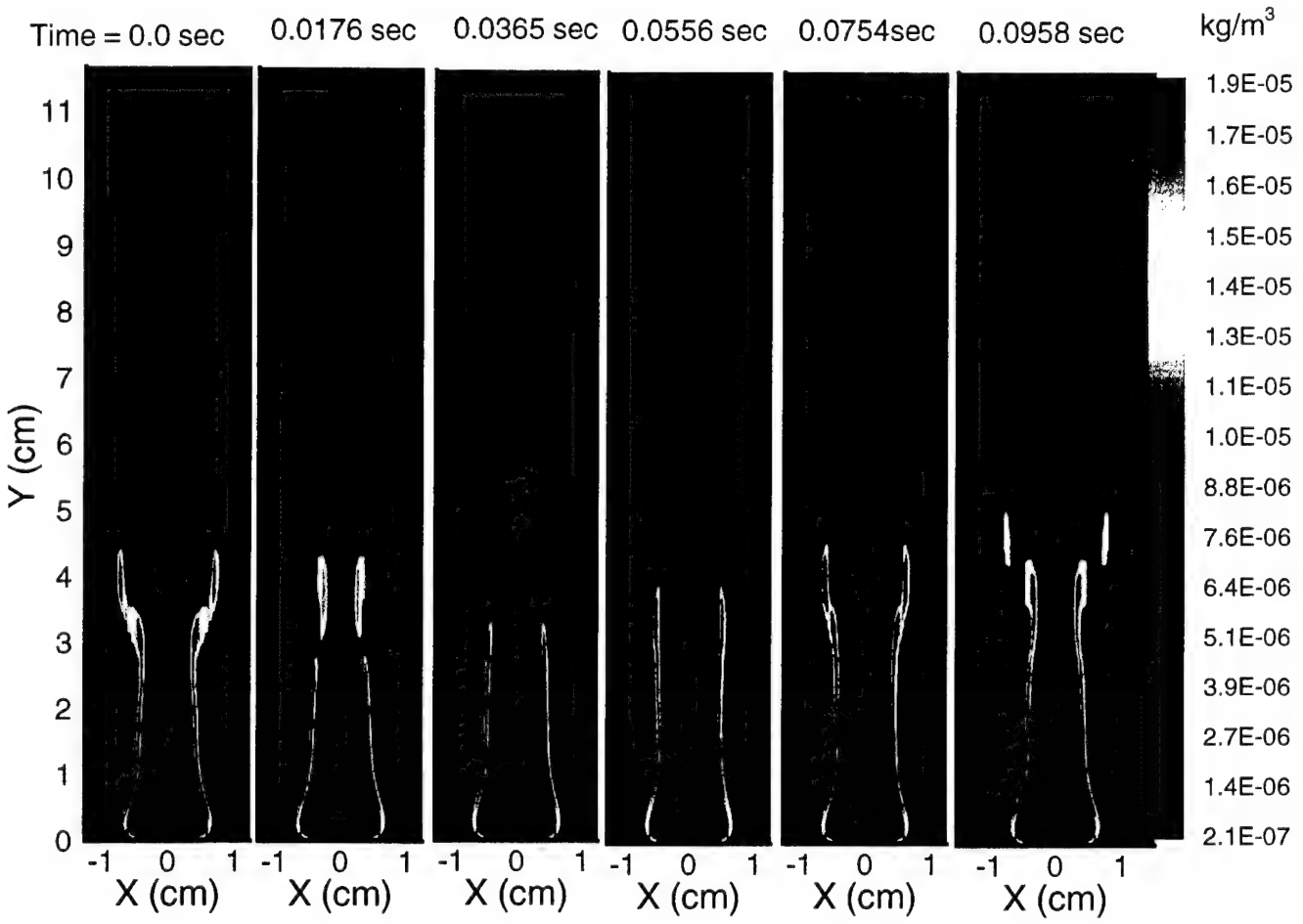


Fig. 4. Time dependent sectional density contours (0-10 $\mu$) for water-mist suppression of methanol pool fire with an air co-flow velocity of 10 $cm/s$. The water-mist (50$\mu$ , 1000 $drops/cm^3$) is injected at the base of the flame.

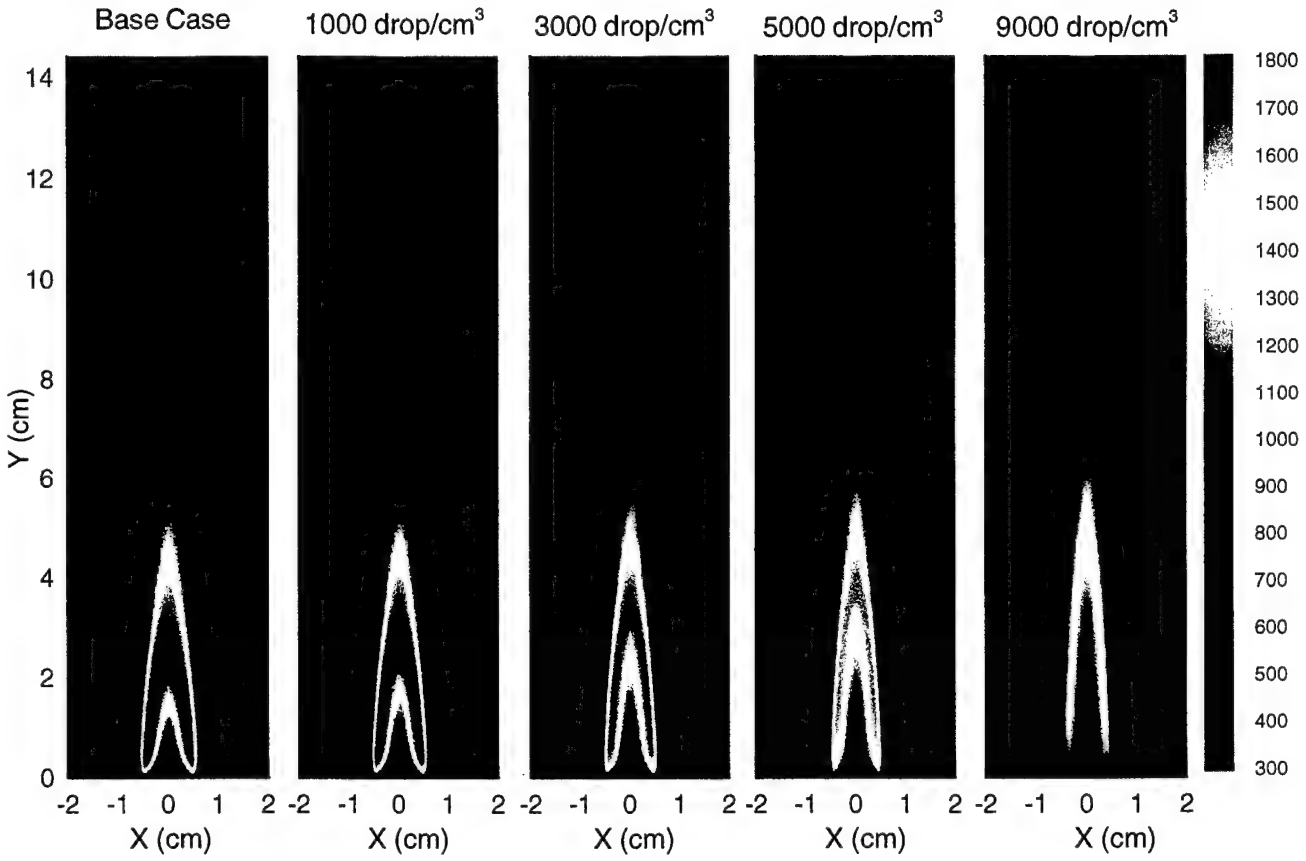


Fig. 5. Typical temperature contours above a methanol liquid pool fire for various droplet injection densities.

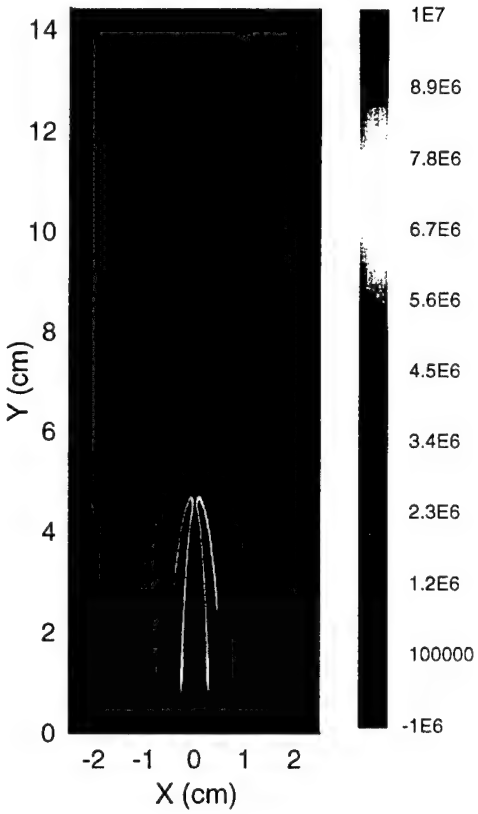


Fig. 6. Typical heat release rate contours above a methanol liquid pool fire for a droplet injection density of 1000 $drops/cm^3$.

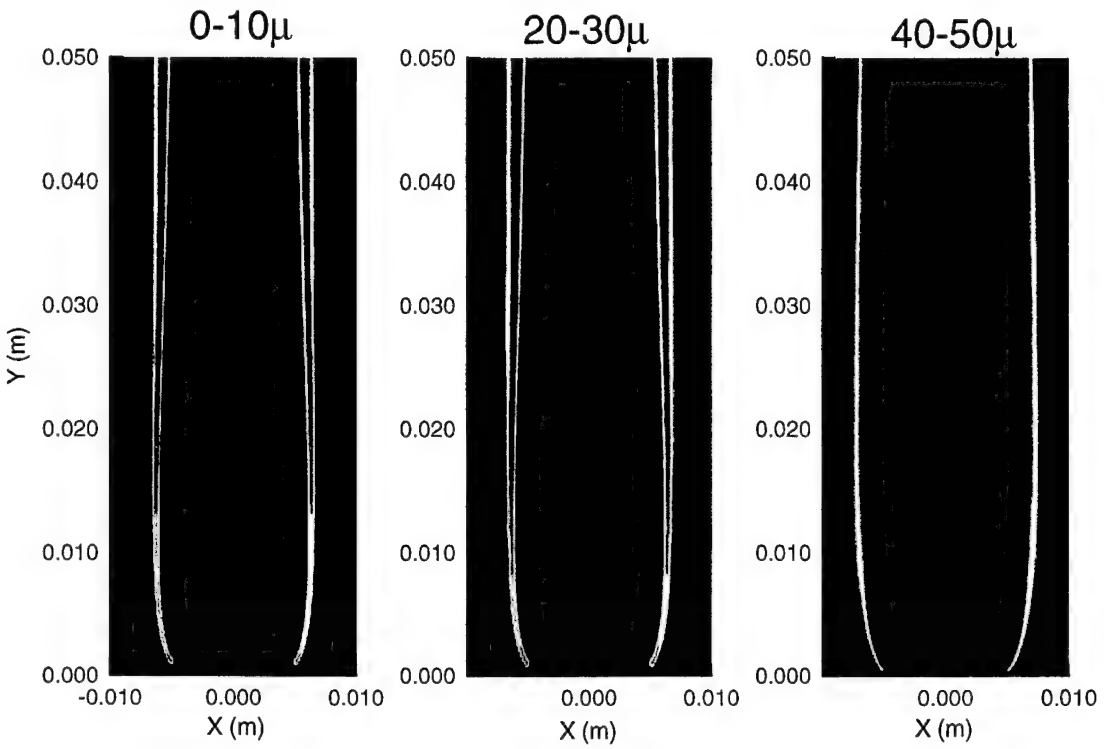


Fig. 7. Sectional density contours during base injection of $50\mu$ droplets on a methanol liquid pool fire.

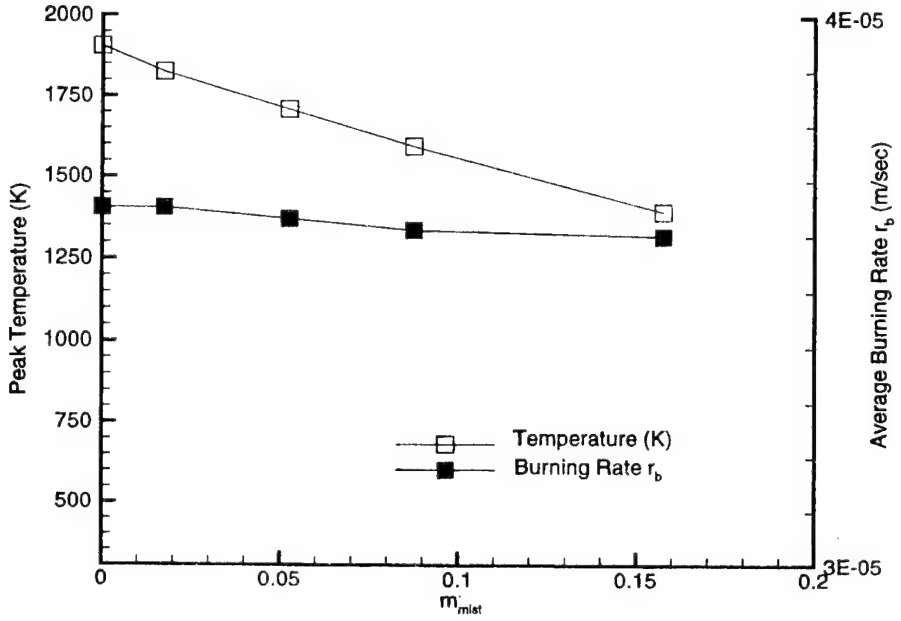


a) 50 $\mu$ water-mist

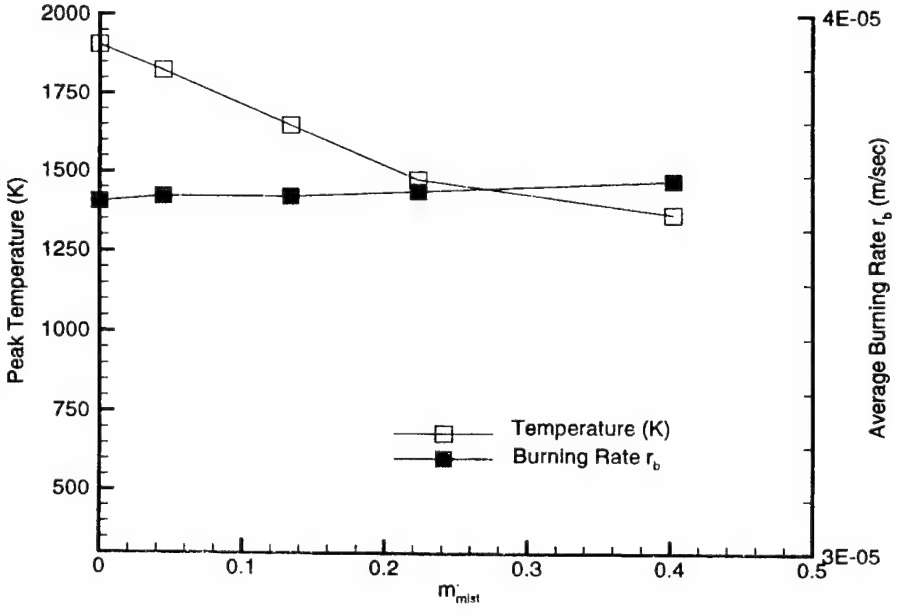


b) 150 $\mu$ water-mist

Fig. 8. Peak temperature vs. injection mass density ($kg/m^2/s$).

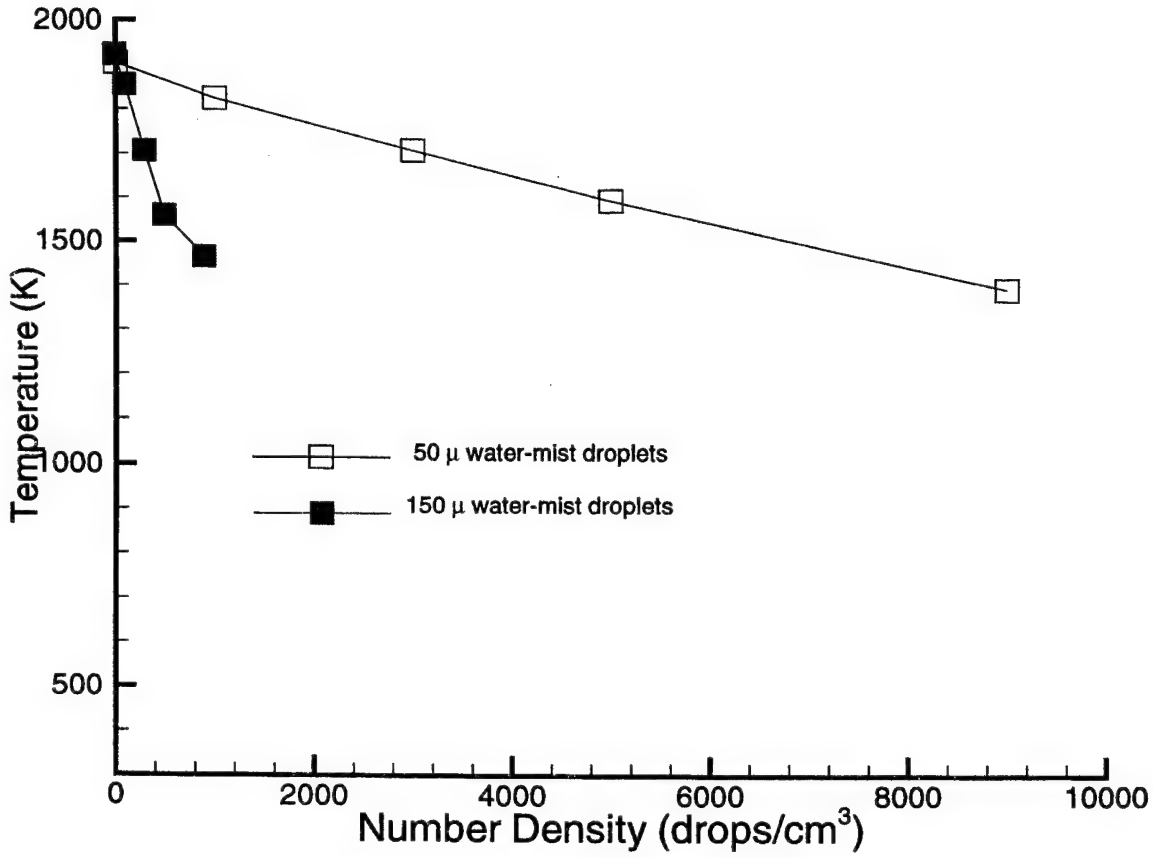


Fig. 9. Peak temperature vs. injection number density

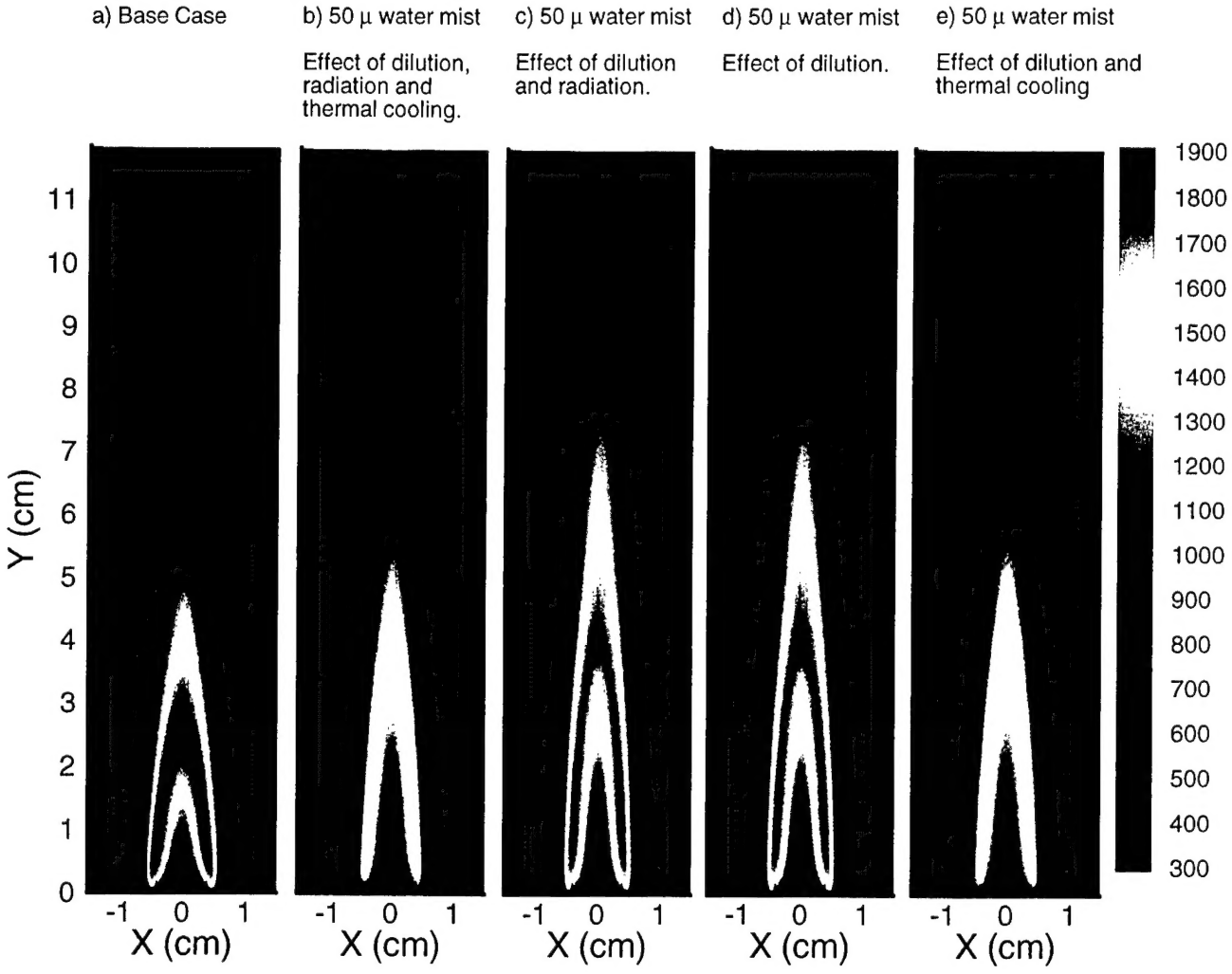


Fig. 10. Temperature contours illustrating the relative contribution of various water-mist suppression mechanisms. a) base case, b) water mist c) water mist with no heat of vaporization d) water mist with no heat of vaporization and no radiation e) water mist with no radiation

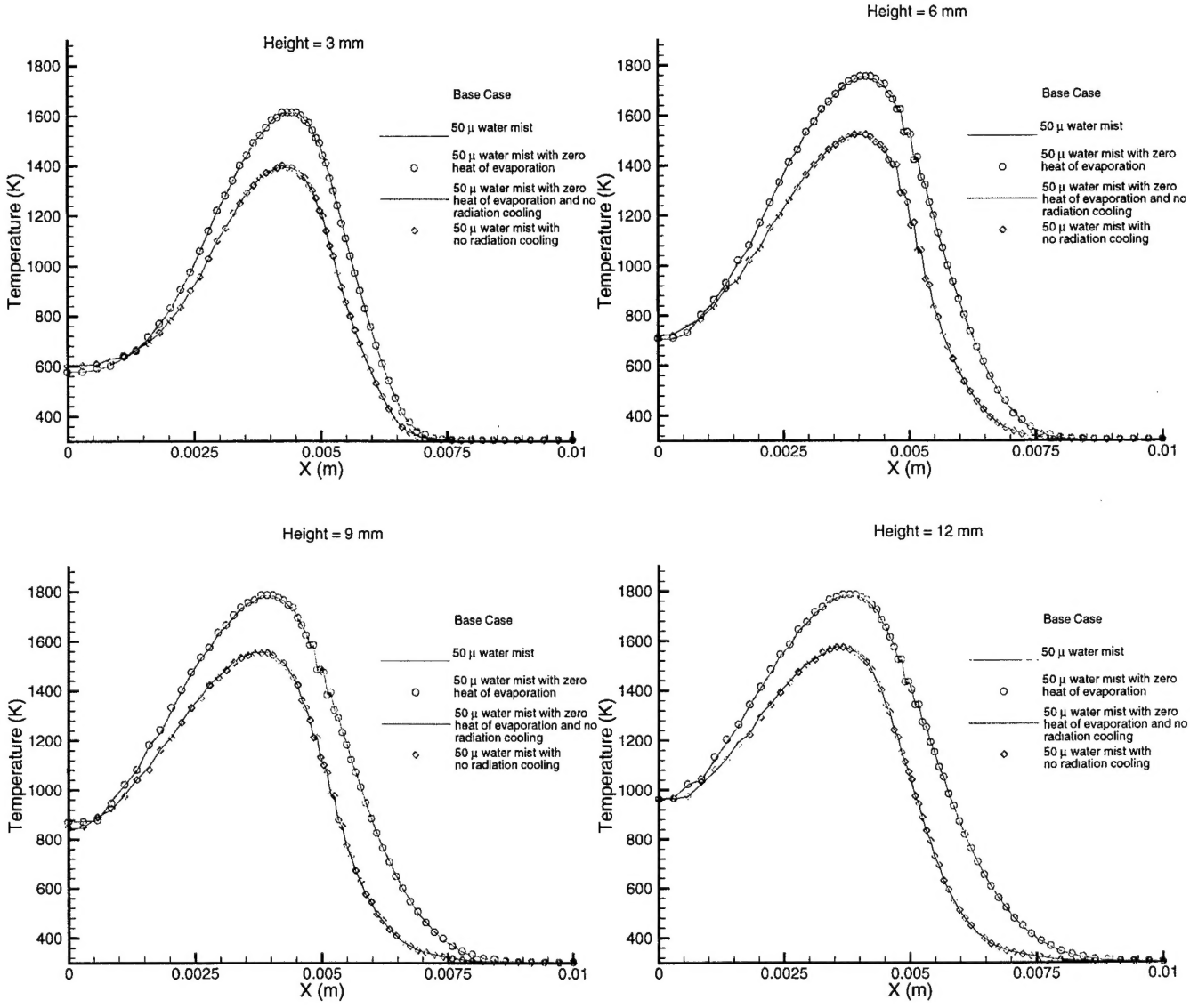


Fig. 11. Relative contribution of various water-mist suppression mechanisms such as thermal cooling, oxygen dilution and radiation attenuation illustrated using temperature profiles for a) base case, b) water mist c) water mist with no heat of vaporization d) water mist with no heat of vaporization and no radiation e) water mist with no radiation

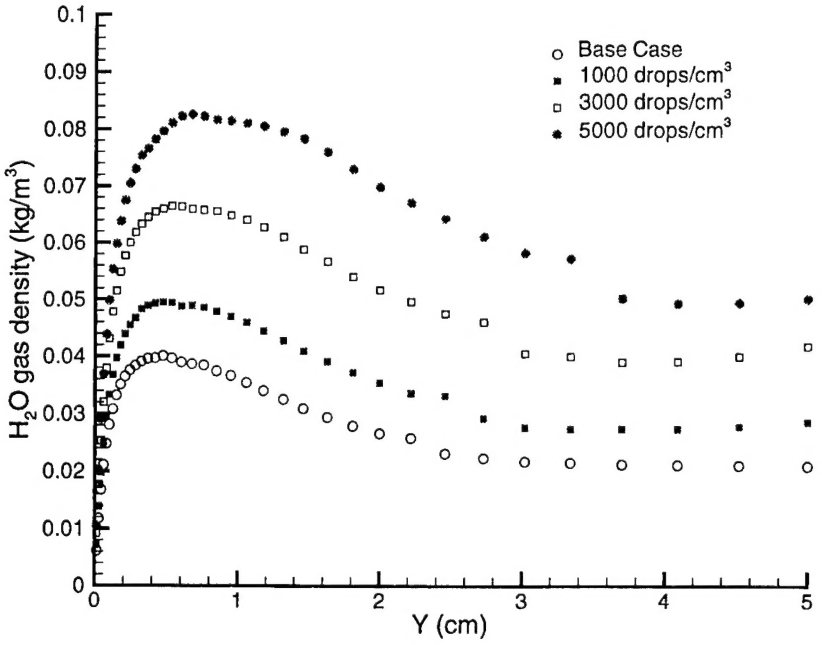


Fig. 12. Center line water-vapor density as a function of distance above the burner surface for various spray injection densities.

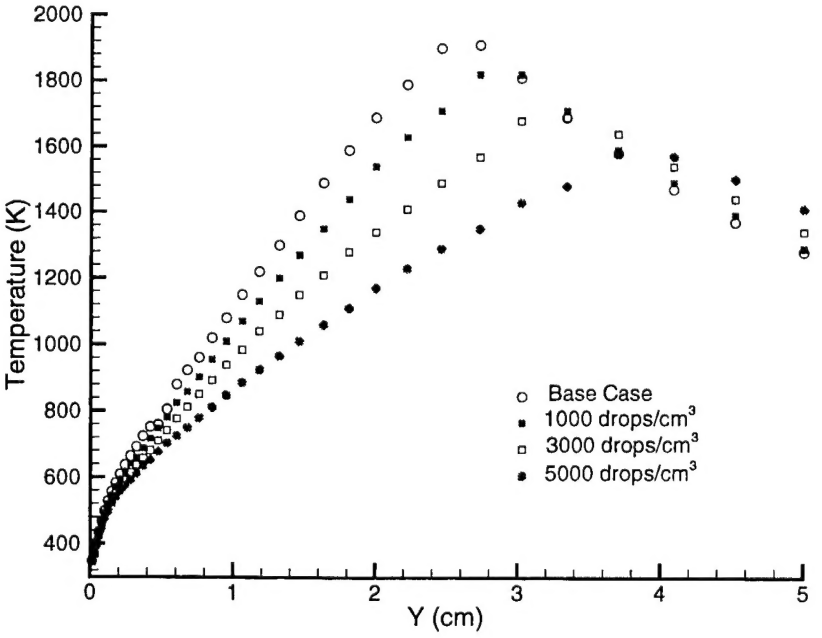


Fig. 13. Center line temperature profile as a function of distance above the burner surface for various spray injection densities.

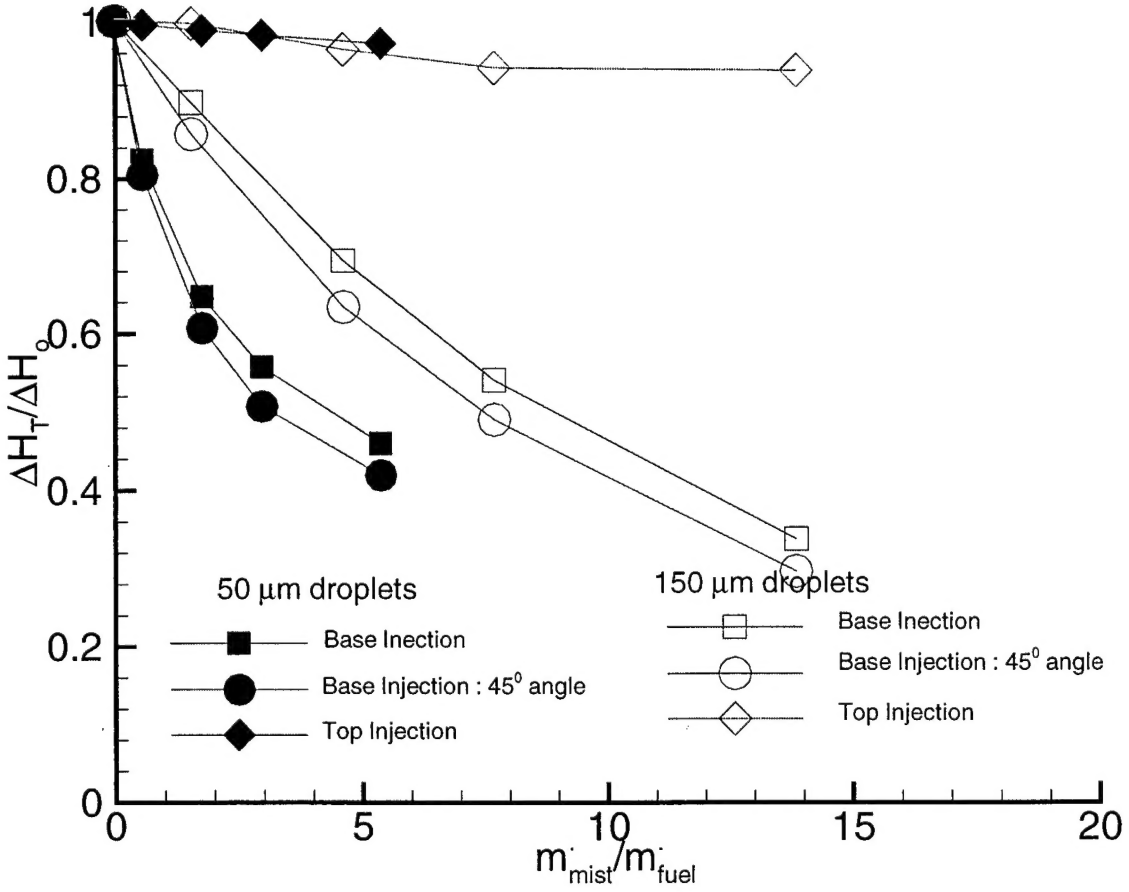


Fig. 14. Net suppression effect of water-mist as a function of water/fuel ratio for base injection, side injection and top injection configuration.